Natural Hazards
and Earth System
Sciences

Open Access

Discussions

EGU

Updated area-source seismogenic model for seismic hazard of Italy

Francesco Visini[1], Carlo Meletti[1], Andrea Rovida[2], Vera D'Amico[1], Bruno Pace[3], Silvia Pondrelli[4]

5   [1]Istituto Nazionale di Geofisica e Vulcanologia, Sezione di Pisa, Pisa, Italy

[2]Istituto Nazionale di Geofisica e Vulcanologia, Sezione di Milano, Milano, Italy

[3]Dipartimento di Ingegneria e Geologia, Università degli Studi di Chieti-Pescara, Chieti, Italy

[4]Istituto Nazionale di Geofisica e Vulcanologia, Sezione di Bologna, Bologna, Italy

10   *Correspondence to*: Francesco Visini (francesco.visini@ingv.it)

Abstract. A new probabilistic seismic hazard model, called MPS19, has been recently proposed for the Italian territory, as a result of the efforts of a large national scientific community. This model is based on 11 groups of earthquake rupture forecast inputs and, particularly, on 5 area-source seismogenic models, including the so-called "MA4" model. Data-driven procedures were followed in MA4 to evaluate seismogenic parameters of each area source, such as upper and lower seismogenic depth,
15   hypocentral depth distributions and nodal planes. In a few cases, expert judgment or ad-hoc assumptions were necessary due to the scarcity of data. MA4 consists of 20 seismicity models that consider epistemic uncertainty in the estimations of the completeness periods of the earthquake catalogue, of maximum magnitude values and of seismicity rates. In particular, 5 approaches were adopted to calculate the rates, in the form of truncated Gutenberg-Richter frequency-magnitude distribution. The first approach estimated seismicity rates using earthquakes located in each source zone, while the other approaches firstly
20   calculated the *a* and *b* values of the truncated Gutenberg-Richter relation for groups of zones considered tectonically homogeneous, and successively partitioned in different ways the *a* values to the zones forming each group.

The results obtained in terms of seismic hazard estimates highlighted that the uncertainty explored by the 20 seismicity models of MA4 is at least of the same order of magnitude of the uncertainty due to alternative ground motion models.

1. Introduction

25   A recent project led by the Seismic Hazard Center (Centro di Pericolosità Sismica, CPS) of the Istituto Nazionale di Geofisica e Vulcanologia (INGV) and funded by the Italian Civil Protection Department produced a new time-independent probabilistic seismic hazard model for Italy, called "Modello di Pericolosità Sismica 2019 - MPS19" (Meletti et al., 2021). The model is constituted by a suite of Earthquake Rupture Forecasts (ERFs) and Ground Motion Models (GMMs), respectively described in Visini et al. (2021) and Lanzano et al. (2020), that are based on updated and new data acquired in the last decades after the
30   release of the current reference Italian seismic hazard model in 2004-2006 (MPS04; Stucchi et al., 2011).

Natural Hazards
and Earth System
Sciences
Discussions

In particular, MPS19 consists of 564 alternative seismic hazard models (i.e. logic-tree branches) obtained by combining 11 groups of ERFs, each made by a different number of sub-models (for a total of 94 ERFs) to consider the epistemic uncertainty inside each group, with a set of 6 GMMs (3 for active shallow crustal regions, 2 for subduction zones and 1 for volcanic areas).

In terms of seismic source typologies, 5 groups of ERFs out of 11 consider area sources, 2 are based on smoothed seismicity
35   calculated on a grid of points, 2 combine faults sources with background seismicity, and 2 derive earthquake rates from geodetic data over a grid of points. The ERFs are based on updated and new historical, geological, and palaeoseismological data sets collected over the last 15 years, after the realization of MPS04, on the Italian territory and its conterminous areas.

In this paper we describe one of the 5 area-source ERFs, that is the so-called "MA4" model (i.e. area-source model #4), developed by updating the data and assumptions underlying the seismogenic model ZS9 (Meletti et al., 2008) adopted in
40   MPS04. MA4 is based on a seismotectonic zoning that we defined as "ZS16" to mark the scientific heritage of the ZS9 model and its previous versions, such as ZS4 (Meletti et al., 2000). In particular, ZS9 resulted from modifications, merges and eliminations of the numerous areas delineated in the previous zoning ZS4, as well as from the introduction of new ones. The goal of ZS9 was to build a model consistent with new data collected at the time of its development. ZS4 was in fact based on the geodynamic model and seismotectonic knowledge available in the first half of the 1990s (Meletti et al., 2000). Since most
45   of that knowledge was considered still reliable during the development of ZS9, this latter was built without introducing drastic elements of novelty as regards the general kinematic framework on which ZS4 was based. In some cases, groups of area sources of ZS4 were merged on the basis of the characteristics of the kinematic domain to which each of the area sources was attributed. In the meantime, the geometry of the area sources was modified according to the changed seismotectonic knowledge. Most importantly, in ZS9 the choice of drawing area sources large enough to include all the seismicity above a
50   certain magnitude threshold, a criterion used in ZS4 as precautionary in terms of hazard assessment, was abandoned. Instead, in the development of MPS04 it was found that, in many cases, the increase in the surface of area sources incorrectly reduced the hazard estimate in the central parts of the area, characterized by the most important earthquakes in terms of magnitude and numbers. ZS9 was then developed by constraining the geometry of source zones with locations of seismogenic faults and of historical and instrumental earthquakes, avoiding arbitrary extensions of the dimensions of the zones. Figure 1 shows the ZS9
55   model, consisting of 36 area sources, together with ZS4.

The seismotectonic zoning ZS16 of the MA4 model incorporates a number of different information for each defined area source: a) geographical boundaries, b) top and bottom depth of the seismogenic layer, c) hypocentre distribution, and d) style of faulting. For each area source, 5 alternative frequency-magnitude distributions were computed, providing the annual rates of all earthquakes with $Mw \geq 4.5$, that is the threshold magnitude adopted in MPS19 (Meletti et al., 2021; Visini et al., 2021).
60   In the following, we first briefly introduce the input data considered for developing the MA4 model, then describe the methods used to define the geometry of area sources and to estimate, for each of them, top and bottom depth of the seismogenic layer, hypocentres distribution, style of faulting, and annual rates of earthquake occurrence. Finally, seismic hazard estimates computed using the MA4 seismicity model are presented and discussed.

2. Input data

65   Area sources for probabilistic seismic hazard assessment (PSHA) represent regions with seismicity spatially uniform in terms of earthquake occurrence rates, maximum magnitude, expected rupture mechanism, and so on. In our model, mapped active faults played a major role in defining the boundaries of the area sources, however we integrated geological data with historical and instrumental seismicity, as well as with geophysical data, including geodetic strain field, maximum horizontal stress (Shmax) orientation and focal mechanisms, to define the geographical borders of the areas, the prevailing style of faulting, the

70   upper and lower bounds of the characteristic seismogenic depth, and the distribution of hypocentral depths.

To determine the boundaries and the seismic parameters of the area sources we collected and analyzed several seismotectonic datasets (Fig. 2), some of which were compiled in the framework of MPS19 (Meletti et al., 2021) to be used as common inputs for the development of all the ERFs. Among these datasets, we used: an historical earthquake catalogue (*Catalogo Parametrico dei Terremoti Italiani* CPTI15, version 1.5, hereinafter CPTI15; Rovida et al., 2016; 2020); an instrumental earthquake

75   catalogue (Gasperini et al., 2016; Lolli et al., 2020); the version 3.2.1 of the Database of Italian Seismogenic Sources (DISS 3.2.1; Basili et al., 2008; DISS Working Group, 2018); an harmonized GPS velocity model for the Mediterranean area (Devoti et al., 2017); and other geological and geophysical data, available for specific regions and for the whole territory, as described in the following.

80   ### 2.1. Earthquake catalogues

CPTI15 v.1.5 lists 4389 earthquakes with moment magnitude Mw ≥ 4.0 or macroseismic intensity ≥ 5 occurred in the Italian and neighboring areas (Fig. 2a) in the period 1000-2014. The catalogue provides epicentral locations and homogeneous Mw estimates derived from both macroseismic and instrumental data. The catalogue takes advantage of the wealth of macroseismic intensity data related to both historical and recent earthquakes collected in the Italian Macroseismic Database DBMI15 (version

85   1.5; Locati et al., 2016). The parameters of the 43% of the earthquakes are calculated from such intensity data with the Boxer algorithm (Gasperini et al., 1999; 2010) with an updated calibration (Rovida et al., 2020). Following Gasperini et al. (2012), instrumental magnitudes are moment tensor solutions complemented with proxy Mw obtained from magnitude estimates in other scales according to Gasperini et al. (2013) and Lolli et al. (2014; 2015; 2018). For the sake of homogeneity, the Mw of modern earthquakes with both macroseismic and instrumental magnitudes is the combination of the two estimates.

90   Specifically, for MPS19, mainshocks were identified in the catalogue according to the declustering procedure by Gardner and Knopoff (1974), which identified 3353 mainshocks, corresponding to the 76% of the whole catalogue.

To define the seismogenic layers and the depth distributions of the earthquakes in the area sources, we also considered an instrumental catalogue with homogeneous Mw determination for the period 1981-2015 (Gasperini et al., 2016). An updated and slightly different version of this catalogue was later published as Lolli et al. (2020), with a thorough description of the

95   input data and selection criteria. The catalogue contains the instrumental part of CPTI15, complementing it for magnitude
<4.0.

2.2. Focal mechanisms

To collect a representative dataset useful to define the styles of faulting of each area source (Fig. 2b), we started from the CMT
100   Italian Dataset (Pondrelli et al., 2006; https://doi.org/10.13127/rcmt/italy; CMT Italian Dataset, 2020). This dataset includes
all available moment tensors for the Italian peninsula and surrounding areas from 1976 with a minimum Mw of 4.0, collected
from the Global CMT (Centroid Moment Tensor; Ekström et al., 2012 and references therein) Catalogue and the Euro-
Mediterranean RCMT (Regional Centroid Moment Tensor) Catalogue (Pondrelli and Salimbeni, 2015;
https://doi.org/10.13127/rcmt/euromed). To reach the best homogeneity in terms of spatial distribution, few M≥4.0 earthquakes
105   occurred in the Alpine region, obtained through seismic data inversions and belonging to the German Research Centre for
Geosciences (GFZ) and ETH Zurich datasets (Saul et al., 2011, and Bernardi et al., 2004, respectively) were added. In addition,
to get a dataset with a longer time-coverage, we considered first polarity focal solutions for relevant events that occurred before
the digital era, such as the 1968 Belice (Sicily) earthquakes. These focal solutions were extracted from the EMMA database
(Database of Earthquake Mechanisms of the Mediterranean Area; Vannucci and Gasperini, 2004). In a few cases, multiple
110   focal mechanisms were available for a single event and their choice followed the quality evaluation given in the EMMA
database where a "preferred" solution is defined (see Pondrelli et al., 2020 for details).

2.3. Active faults

The DISS database (Basili et al., 2008; DISS Working Group, 2018) is a fundamental product for interpreting the relationships
115   between faults and earthquakes in Italy. DISS 3.2.1 contains 127 Individual Seismogenic Sources, 188 Composite Seismogenic
Sources (defined as simplified and three-dimensional representations of crustal faults containing an unspecified number of
seismogenic sources that cannot be singled out, Fig. 2c), 35 Debated Seismogenic Sources, and 3 subduction zones. All sources
are based on geological/geophysical data and cover the whole Italian territory and portions of adjacent countries and seas.
At the national scale, we also considered the "Structural Model of Italy" (CNR, P.F. GEODINAMICA 1990) and the
120   seismotectonic model by Meletti et al. (2000). The latter was used as a guide for identifying homogeneous domains of active
tectonics in Italy.
In some regions, we integrated the above datasets with data from local detailed geological-structural investigations to define
the boundaries of the area sources, for example: Delacou et al. (2004) and Sue et al. (2007) for northwestern Italy; Collettini
and Barchi (2002), Boncio et al. (2004), Papanikolaou and Roberts (2007), Lavecchia et al. (2007a), Faure Walker et al (2010;
125   2012), Visini (2012), Tesson et al. (2016) and Valentini et al. (2017) for central and southern Italy; Lavecchia et al. (2007b),
Catalano et al. (2010), Billi et al. (2010), Visini et al. (2010) and Mastrolembo et al. (2014) for Sicily.

2.4. Other geophysical data

As a proxy for evaluating the thickness of the crust and defining zones with similar seismogenic thickness, we used the Moho
130 maps by Solarino and Cassinis (2007) and Di Stefano et al. (2011), and the heat flow maps by Della Vedova et al. (2001).
We also considered the regional strain rate fields for the Mediterranean area derived from GPS data (Devoti et al., 2017) and
the maximum horizontal stress Shmax orientation (Mariucci and Montone, 2020) to qualitatively check the homogeneity of
the strain rate values within the area sources.

3. The MA4 seismogenic model

135 ### 3.1 The ZS16 seismotectonic zoning

Although area sources are widely used for national and international PSHA, there are no standard objective approaches for
defining their boundaries. We acknowledge the criteria defined in previous studies (e.g. Giardini, 1999; Meletti et al., 2008;
Wiemer et al., 2009; Vilanova et al., 2014; Danciu et al., 2018) to set guidelines for the delineation of area sources in order to
describe the correlation between active faults, earthquakes and other geophysical inputs. To update the existing reference
140 national zoning scheme ZS9 we applied the following criteria:

- a) start from the area sources of the ZS9 model;
- b) be consistent with the general background delineated by the geodynamic model proposed by Meletti et al. (2000), i.e. an area source should contain a unique tectonic zone (active shallow crustal, volcanic or subduction zone in the specific Italian case);
- 145 c) incorporate all recent advances in the understanding of the active tectonics of the territory and in the distribution of seismogenic sources modelled in the DISS 3.2.1 database and other active fault compilations at the national and regional scale (see section 2.3);
- d) incorporate information derived from the investigation of the most recent seismic sequences that struck Italy after the compilation of ZS9, namely the L'Aquila 2009, Emilia 2012 and Amatrice-Norcia 2016 sequences;
- 150 e) be consistent with the CPTI15 earthquake catalogue;
- f) define area source boundaries that primarily follow the surface projection of mapped active faults: an area source should not interrupt a normal or reverse fault system unless major differences are observed (changes in stress orientation and/or changes in crustal depth); for strike-slip faults, boundaries should be parallel to the strike of the faults and the area source should contain the faults;
- 155 g) consider for the definition of the boundaries: the pattern of seismicity, focal mechanisms, geodetic strain field, Shmax and heat flow data;

h)   account for the variation of the style-of-faulting and tectonic regime with depth, therefore multiple area sources can overlap on the volume domain;

i)   cover the entire Italian territory, as required by MPS19.

160   Applying these criteria to the data described in section 2, we defined the seismotectonic zoning shown in Figure 2d, consisting of 48 active shallow crustal area sources and 2 area sources corresponding to the Campanian and Mt. Etna volcanic districts (i.e., area sources #31 and #49, respectively). For the deep seismicity related to the Thyrrenian subduction intraslab, no area sources were defined, because MPS19 adopted a separate ad-hoc ERF for modelling such seismicity. Finally, it is worth noting that 3 area sources (#19, #20 and #25) showed a different kinematics for shallow and deep seismicity (see Pondrelli et al., 2020

165   for details).

3.2. Top and bottom depth of the seismogenic layer and hypocentral distributions

Seismogenic depths for each area source of ZS16 were estimated using the instrumental catalogue by Gasperini et al. (2016). In particular, we assumed the upper and lower limits of the seismogenic layer as corresponding to the 5th and 95th percentiles of the depth distribution of the earthquakes inside each area (e.g., Boncio et al., 2009; Stucchi et al., 2011), and the prevalent

170   hypocentral depths as the modal values of this distribution.

To estimate these values, we first removed the earthquakes with fixed hypocentral depth (i.e. 0, 5 or 10 km), that represent ~10% of the total. We then considered only the earthquakes that can be related to active crustal seismicity based on the crustal models by Solarino and Cassinis (2007) and Di Stefano et al. (2011). In the Mt. Etna region, we assigned earthquakes with hypocentral depth < 10 km to the volcanic domain (area source #49 in Fig. 2d) and earthquakes with hypocentral depth ≥ 10

175   km to the underlying active crustal area sources (#44, #45, and #46). For the Campanian volcanic area (#31 in Fig. 2d), we adopted depth values of 0 km, 4 km and 1 km, respectively for the top and the bottom of the seismogenic layer and for the prevalent hypocentral depth, mainly based on the parameters of the 2017 Mw 3.9 Ischia earthquake (De Novellis et al., 2018). We then divided area sources #19, #20 and #25, showing a different kinematics for shallow and deeper seismicity (Pondrelli et al., 2020), into "shallow" and "deep" zones. Basing on crustal thickness and rheological properties, we adopted ad hoc

180   values of depth for these zones: for shallow zones, we assumed depth values of 0 km, 15 km and 10 km, respectively for the top and the bottom of the seismogenic layer and for the prevalent hypocentral depth; for deep zones, we assumed depth values of 15 km, 30 km and 23 km, respectively for the top and the bottom of the seismogenic layer and for the prevalent hypocentral depth. For all the other area sources, we calculated the 5th and 95th percentiles of the hypocentral depth distributions, respectively assumed as the upper and lower limits of the seismogenic layer. For depths within these limits, we then computed

185   modal values, standard deviation and log-likelihood of the unimodal and bimodal distributions that best fit the observed values. We evaluated and compared the AIC (Akaike Information Criterion) index of the unimodal and bimodal distributions to select the best model for the hypocentral depth distribution of each area. In case of unimodal distribution, we used the modal value as representative of the prevalent hypocentral depth, while for bimodal distributions, we assigned weights to both modal values by using their mixing proportion value in the bimodal distribution. To evaluate the stability of the results with respect to the

190 number and the magnitude of the considered events, we calculated the upper and lower seismogenic depths and the modal values of the distributions for different minimum magnitudes (from Mw 2.5 to 4.5), and compared the resulting depth estimates with the depth of the composite seismogenic sources of DISS 3.2.1 inside the area. In Figure 3, we show an example of the results obtained for zone #24. Electronic supplement 1 lists the parameters derived for all the area sources for minimum magnitude Mw 2.5, which resulted to be the most appropriate threshold value to ensure a significant number of earthquakes

195 for all the areas.

3.3 Style of faulting

Pondrelli et al. (2020) defined the criteria to parametrize the styles of faulting of expected earthquake ruptures and to evaluate their representativeness in each area source. Using available seismic moment tensors for relevant events (Mw ≥ 4.5), first arrival focal mechanisms for less recent earthquakes, and also geological data on past activated faults, we collected a database

200 for the last ~100 years by gathering thousands of data for the Italian peninsula and regions around it, as described in section 2.2. From this dataset, in each source zone we obtained a representative moment tensor and identified the possible nodal plane(s), considering the different percentages of styles of faulting, and including, where necessary, total or partial random source contributions. As stated above, in a few cases, changes in tectonic style with depth were identified (area source #19, #20 and #25). Figure 4 shows a map with the resulting styles of faulting, reported also in the electronic supplement 2.

3.4. Annual rates of earthquake occurrences

To estimate the expected seismicity rates of each area source, we adopted a time-independent (i.e. Poisson) model for earthquake occurrence. We assumed that the distribution of the earthquake magnitudes follows the Truncated Gutenberg-Richter (TruncGR) model that has two parameters: the upper (or maximum) magnitude (Mu) and the slope (β, β = 2/3 b). The TruncGR distribution is the Pareto distribution with the probability density function truncated at both ends. Its cumulative

210 density function related to the moment magnitude is:

$$\Lambda(M) = \Lambda_0(\exp(-\beta M_0) - \exp(-\beta M))/(\exp(-\beta M_0) - \exp(-\beta Mu)) \tag{1}$$

where $\Lambda(M)$ is the cumulative number of earthquakes per unit time equal to or larger than the magnitude threshold (M_0) and

215 smaller than Mu. β and Λ_0 were derived from the declustered CPTI15 catalogue (see section 2.1) by adopting the completeness time intervals and the maximum magnitude values described in the following and applying a maximum-likelihood fit based on Weichert (1980).

3.4.1. Completeness time intervals

Two independent sets of completeness time intervals for the CPTI15 catalogue were defined according to i) the historical

220 approach of Stucchi et al. (2004; 2011), and ii) the statistical method proposed by Albarello et al. (2001).

The historical approach determines the complete intervals analyzing the local history of a set of sample localities. Based on such a knowledge, the years from which it is unlikely that earthquakes effects of a given intensity are not recorded in the local historical sources were determined. The catalogue can be considered as complete for earthquakes of the same epicentral intensity I0 located at or near the analyzed locality. The completeness threshold and periods assessed for the sample localities

225 were then extrapolated to the area sources they belong to and to others with similar history and seismotectonic features (Stucchi et al., 2004; 2011). Being the approach independent from the catalogue, we applied the same completeness intervals of Stucchi et al. (2011), adapting the 5 macro-regions defined therein to ZS16 and adding one off-shore region (Fig. 5a). In addition, we redefined the Mw bins according to the new empirical conversion relation between epicentral intensity and magnitude of CPTI15 (Rovida et al., 2020) and evaluated the completeness intervals for I0<6, which were not assessed in Stucchi et al.

230 (2011). Completeness intervals were estimated for Mw bins of 0.23 Mw units (Table 1), to avoid the oversampling of some Mw intervals that contain values derived from the conversion of more than one discrete epicentral intensity value.

The statistical completeness intervals were assessed using the procedure of Albarello et al. (2001) for the same macro-regions defined for the historical approach. To ensure the stability of the results, we considered magnitude bins of 0.46 Mw units, which means grouping in the same class integer and intermediate intensity values (e.g. intensity 6-7 together with 6). The

235 results were then applied to the same bins of 0.23 Mw units defined for evaluating the historical completeness (Table 2).

3.4.2. Maximum magnitude

For the definition of the maximum magnitude we used the estimates provided for MPS19, described in Visini et al. (2021). The Italian area was divided into 18 tectonic domains (Fig. 5b) and the earthquakes listed in CPTI15 were assigned to them, according to their location. Based on the average error of magnitude estimates for earthquakes occurring before and after 1980,

240 a minimum value of uncertainty for the Mw evaluation of 0.3 and 0.2 was introduced for the historical and instrumental portion of the catalogue, respectively. The maximum observed magnitude inside a tectonic domain is the largest magnitude observed, including the uncertainty ("Mwobs+uncertainty"). Then, following Woessner et al. (2015), a minimum value of Mwmax was assigned to each tectonic domain (Mwtect), namely 6.5 for all active crustal areas, 6.0 for the Tyrrhenian tectonic domain, and 5.6 for the volcanic area of Etna. Two values of maximum magnitude were then assigned to each tectonic domain: i) Mwmax1

245 (Figure 5c), that is the largest value between Mwtect and Mwobs+uncertainty, and ii) Mwmax2, that results by uniformly incrementing Mwmax1 by a cautionary value of 0.3 to account for epistemic uncertainties, except for the Etna volcanic domain where Mwmax2 is equal to Mwmax1. The two values of Mwmax were also checked with the estimates of the maximum Mw of the composite seismogenic sources of DISS 3.2.1 inside each tectonic domain (see Visini et al., 2021 for details).

3.4.3 Seismic rates determination

250 To calculate annual rates of earthquake occurrences for the active shallow crustal areas, we first excluded from the CPTI15 the events belonging to the Southern Thyrrenian subduction (i.e. those located in that area with hypocentral depth larger than

Natural Hazards
and Earth System
Sciences
Discussions

40 km), and we imposed a minimum of 10 earthquakes and at least 2 non-empty classes of magnitude (0.1 bin size) in each area source to derive stable β values; otherwise, we assumed β equal to 2.3 (b =1).

255 We used 5 different approaches to calculate the seismicity rates for the area sources, which are based on 2 different assumptions. The first assumption is that β varies across the areas, then a first approach (named, approach i) consists in the classical estimation of the parameters $\Lambda(M)$ and β (see Eq. 1) directly for the area sources. The second assumption is that β is stable over groups of zones with similar seismotectonic features. Under the latter assumption, we first calculated β for groups of area sources, hereinafter defined as "macroarea", then we partitioned $\Lambda(M)$ to the sources belonging to the same group. To this purpose, we used the tectonic domain shown in Figure 5b

260 As the next step, we assessed the recurrence parameters in each source zone within a macroarea. Keeping with our objective to only change $\Lambda(M)$ according to the level of seismic activity of an area, we defined 4 different methods for partitioning $\Lambda(M)$. In particular, defined $\Lambda(M)$as and $\Lambda(M)$ma respectively as the values of $\Lambda(M)$ of the area source and of the macroarea:

ii) we calculated the average ratio of the observed rates of occurrence of all the areas with respect to the macroarea they belong to and then used these ratios to scale $\Lambda(M)$ma to $\Lambda(M)$as;

265 iii) we anchored $\Lambda(M)$as to the threshold magnitude Mt of the respective area source and then normalized $\Lambda(M)$as to sum to $\Lambda(M)$ma;

iv) we calculated $\Lambda(M)$as to maximize the log-likelihood of the observed and forecasted number of earthquakes in each AS;

v) we calculated the $\Lambda(M)$as that minimizes the root-mean-square of the observed rates of occurrence in each AS.

For the areas #19, #20 and #25, we successively partitioned the 5 $\Lambda(M)$as between the "shallow" and "deep" sources, according

270 to their relative percentage of number of earthquakes with Mw≥2.5.

Figure 6 shows an example of the frequency-magnitude distributions calculated directly for the area sources #17, #18, #23 and #24 and the distributions calculated for the macroarea #6 and then partitioned to the same sources. In the electronic supplement 3 we listed the parameters of the TruncGR distributions associated with each area source.

4. Seismic hazard estimation using MA4

275 Seismic hazard was calculated over the whole Italian territory (including sites located within 5 kilometers outside the borders) adopting the MA4 seismogenic model. To this purpose, 52 area sources were used, considering the zones #19, #20 and #25 in the form "shallow" and "deep" and discarding the source #49 (Etna). In fact, for the MS19 model, all ERFs (included MA4) were integrated with 3 ERFs developed ad hoc (see Meletti et al., 2021; Visini et al., 2021) for: a) the Etna volcanic area; b) the subduction shallow interface seismicity and deep intra-slab seismicity of the Calabrian Arc (spanning from the Ionian Sea

280 to the southern Tyrrhenian Sea across the Calabria region); and c) the seismogenic sources located outside the area of the CPTI15 catalogue.

Alternative choices and interpretations about the key elements were embedded in a logic-tree structure (Kulkarni et al., 1984; Coppersmith and Youngs, 1986; Senior Seismic Hazard Analysis Committee, 1997), that is the conventional tool to capture

the epistemic uncertainty associated with the input elements of a PSHA model. The adopted logic tree, shown in Figure 7,
consists of a first branching level accounting for the 2 alternative evaluations of the catalogue completeness time intervals
described in section 3.4.1, i.e., one based on historical information (Stucchi et al., 2004; 2011) and one on the statistical
approach by Albarello et al. (2001). Then, a second branching level considers the 2 alternative sets of maximum magnitude
Mu (eq. 1) values (i.e. Mwmax1, Mwmax2), described in section 3.4.2, and a third level accounts for the 5 approaches adopted
for calculating the frequency-magnitude distributions of each area source (see section 3.4.3). Since we have no specific reason
to prefer or to differently weight the 20 resulting ERF branches, the same weight (i.e., 1/20) was assigned to each of them.
Following Woessner et al. (2015) and Danciu et al. (2018), we considered the uncertainties on hypocentral depths and focal
mechanisms as aleatory. Two further branching levels account for alternative choices of GMMs, as selected and applied in
MPS19 (see Lanzano et al., 2020 for details), that are 3 GMMs for active shallow crustal regions (Bindi et al., 2011; Bindi et
al., 2014; Cauzzi et al., 2015, with associated weights equal to 0.45, 0.32 and 0.23, respectively), and 1 GMM for volcanic
areas (Lanzano and Luzi, 2020). The selected GMMs provide estimates of ground shaking in terms of the geometric mean of
the horizontal components. As a result, we obtained a final logic tree made of 60 branches (Fig. 7).

Seismic hazard was calculated by the OpenQuake engine platform (Pagani et al., 2014). We recall here that, for the computation
of seismic hazard, OpenQuake discretizes every area source into a regular grid of points, each representing the longitude and
latitude of the centre of a rupture. Every rupture has a rectangular shape and is centred on the hypocentral distribution
parameterized in ZS16. Ruptures are created by conserving the area computed from the corresponding value of magnitude
using the magnitude-area scaling relationship of Wells and Coppersmith (1994) and an aspect ratio of 1. The annual rates of
earthquake occurrences of MA4 are given as a non-cumulative magnitude-frequency distribution.

Figure 8 illustrates the spatial distribution of mean Peak Ground Acceleration (PGA) values obtained by applying the weighting
scheme in Figure 8, for 10% and 2% probabilities of exceedance in 50 years. The map for PGA at 10% probability of
exceedance in 50 years (Fig. 8a) shows the highest hazard estimates (PGA≥0.25 g) in 3 areas, i.e., in the northeast of Italy,
along the central Apennines, and the southern Apennines. Hazard levels ranging between 0.1 g and 0.25 g characterize the
majority of coastal areas of the Adriatic and Tyrrhenian seas, the southern part of Po Plain, Sicily, and large parts of southern
Italy. The northwest of Italy, Sardinia and part of Apulia show hazard values generally lower than 0.075 g.

The map for PGA at 2% probability of exceedance in 50 years (Fig. 8b) shows that PGA≥0.5 g characterizes almost entirely
the Apennines, part of the southern Po Plain and the northeast of Italy. The southeast of Sicily shows hazard levels ranging
between 0.3 g and 0.5 g, whereas PGA ranging between 0.2 g and 0.3 g characterizes the rest of Sicily and the majority of
Adriatic and Tyrrhenian coastal areas. Hazard levels lower than 0.1 g result in the northwest of Italy, in the southern part of
Apulia and in Sardinia.

Figures 9 and 10 respectively show hazard curves for PGA and Uniform Hazard Spectra (UHS) for accelerations from 0.1 s to
4 s for the cities of Milano, L'Aquila, and Siracusa (see locations in Fig. 8). We chose these cities because they lie in different
tectonic settings and are located inside area sources characterized by different levels of seismic activity. Figure 9 illustrates
the variability of the expected ground motions in PGA, showing the mean hazard level (black line), the hazard curves resulting

from each of the 60 realizations (grey lines) and the uncertainties expressed through the 16th and 84th percentiles (red lines). Figures 10 show the mean and the 16th and 84th percentiles of UHS for 10% and 2% probability of exceedance in 50 years.

320   Figure 11 shows the spatial distribution of the coefficient of variation (CoV) of PGA values for 10% and 2% probabilities of exceedance in 50 years. The CoV is the (weighted) standard deviation divided by the (weighted) mean. CoVs < 0.2 cover a large part of the Italian territory, indicating a low uncertainty in the expected acceleration. CoVs > 0.2 characterize the areas with the lowest PGA and the southeastern sector of Sicily. The latter corresponds to the source zones where the b values show the largest differences between the macroarea and the single-zone approaches.

325   The CoV values in Figure 11 contain uncertainty related both to the ERF and to the GMMs. We then investigated the "magnitude" of both components of epistemic uncertainty at the 3 selected localities. For each site, hazard curves for PGA were plotted by distinguishing the 3 groups composed of 20 of 60 realizations that use the same GMM for active shallow crustal regions. In Figure 12, the 3 groups are shown by red lines for the realizations that adopt Bindi et al. (2011), light-green lines and blue lines for those using Bindi et al. (2014) and Cauzzi et al. (2015), respectively; also, the mean Annual Probability of Exceedance (APOE) for the 3 groups are reported. It can be seen that most of the seismic hazard curves from the different

330   GMMs are overlapping, and the uncertainty due to the GMMs is of a similar order of magnitude as the uncertainty related to the ERF. For Milano and L'Aquila, the mean curves of the 3 groups overlap in a wide range of APOE, especially for APOE < 1e-3. For Siracusa the Bindi et al. (2011) group intersects the Cauzzi et al. (2015) one at APOE of ~ 6e-3; for PGA < 0.04 g, the realizations returning the highest APOE are those using the latter GMM and the realizations returning the lowest APOE are those using Bindi et al. (2011). This rank is inverted for PGA > 0.04 g or APOE < ~ 6e-3.

335   For each PGA value at which APOE was computed, we estimated the mean exceedance probability and its standard deviation, thus yielding pairs of mean APOE and CoV for each PGA level. Figure 13 illustrates the variation of mean APOE with CoV for the 3 sites when: a) both ERF and GMM uncertainties are considered (black solid line), b) only ERF uncertainty is considered and, c) only GMM uncertainty is considered. To analyse the ERF uncertainty, we calculated the mean APOE and

340   CoV of the branches that use the same GMM: the 3 solid lines without symbols (red, green and blue) are obtained by selecting, respectively, branches with Bindi et al. (2011), Bindi et al. (2014), and Cauzzi et al. (2015). To analyse the GMM uncertainty, we calculated mean APOE and CoV of the branches that use the same approach for completeness estimate (statistical [S] or historical [H]), maximum magnitude ([Mwmax1] or [Mwmax2]) and seismic rates of the zones ([AR1]-to-[AR5]): the lines with symbols represent the 20 branches of the ERF.

345   Although the scatter in the results for the different sites and PGA levels, we observe that the total CoV curve (black solid line, labeled "all" in Fig. 13) tends to increase as the exceedance probability decreases at L'Aquila and Siracusa, whereas it is quite stable around 0.3 in Milano. In the case of L'Aquila and Milano there is a clear trend that ERF uncertainty gives larger CoV than GMM uncertainty, for APOE < ~3e-2. This trend holds for Siracusa for APOE > ~3e-3, whereas ERF and GMM uncertainties have similar CoV for lowest APOE.

350   The branches of the ERF that use a highest maximum magnitude (Mwmax2) generally tend to return a higher CoV than the ones with Mwmax1 at lowest APOE, although this is evident for Siracusa but less clear for L'Aquila. For Milano, the trend of

the curves will probably be similar but, due to the lower level of seismic activity, it is not visible in the figure. The other sub-groups of ERFs do not seem to show any systematic trend, suggesting that they do not contribute to propagating uncertainty in the GMMs.

5. Discussion and Conclusions

355

The MA4 seismogenic model is part of a community-based effort that led to the development of a new seismic hazard model for Italy (MPS19; Meletti et al., 2021). MPS19 adopted 11 ERFs, each composed of a number of alternatives that explore the epistemic uncertainty of seismicity modelling (see Visini et al., 2021). In this framework, MA4 represents one of the 5 area-source seismicity models included in the set of ERFs.

360 In Italy a first challenge for the construction of a zone-based source model is the variety of seismotectonic environments, which include spatial and depth variations of the main style of faulting. We defined a list of criteria to this aim, but we cannot exclude that the proposed zoning still contains some a priori bias or, simply, some zones do not reflect the "true" tectonics. Objective criteria to delineate area sources with a quality ranking of the basic data would be an additional step (e.g. Wiemer et al., 2009; Vilanova et al., 2014).

365 As an example, the debate on "large" vs "small" areas concerns subjective choices. "Small" areas are designed to capture changes in seismicity at the local scale (e.g. < 20 km) but, in our opinion, these changes are better highlighted with fault-based models or a smoothed seismicity approach. Our idea of zoning aims at individuating the areas that have a homogeneous behaviour from a seismotectonic point of view, focusing on the similarities rather than on the differences. The experience in seismogenic zoning in Italy since the early 1990s (e.g. the ZS4 model by Meletti et al., 2000) suggests that small source zones, 370 such as to represent single faults, can be appreciated by structural geologists, but make defining their earthquake recurrence parameters very difficult because of the lack of available data that can even produce apparent differences in seismicity distribution at the local scale. Nevertheless, the size of an area source delineating a pattern of high seismicity should be sufficiently small, otherwise the high rate of seismicity is distributed over a larger zone and thus is dangerously reduced due to the effect known as "spatial smearing" (National Research Council, 1988). Therefore, seismic hazard results are different if 375 the same quantity of seismicity is assigned to sources of different size: the smaller the source area, the higher the resulting hazard estimates, and vice versa.

The MA4 model is based on an update (ZS16) of the previous seismotectonic zoning ZS9 (Meletti et al., 2008) adopted by the current Italian reference seismic hazard model MPS04 (Stucchi et al., 2011). ZS16 was recently used in a new European Seismic Hazard Model (ESHM20) as the reference area source model for Italy (Danciu et al., 2021). To determine the activity 380 rates of source zones from earthquake data we initially used the concept of macroarea to evaluate some parameters, such as the maximum magnitude and the b-value of the GR relation, which were then assigned to all the zones belonging to the macroarea. This approach serves to prevent biased spatial variations of b-value due to poor datasets. The uncertainty in magnitude and epicentral location was assumed to be minimal with respect to the other sources of uncertainty in the estimation

385 of seismic hazard, such as maximum magnitude, completeness time intervals or the choice of the GMMs. However, uncertainty related to the magnitude-location-depth estimation of the earthquakes propagates throughout the evaluation of the completeness periods and thus impacts the estimation of seismic rates. We then encourage future studies to account for such uncertainty propagation.

MA4 explored a range of sources of epistemic uncertainty and is constituted by 20 alternative ERFs, that consider different options in terms of completeness time intervals, maximum magnitude and earthquake rates estimation. We observed that the 390 uncertainty related to this set of ERFs is comparable or even higher than the uncertainty related to alternative GMMs. Although this observation is not generalizable to other ERFs, it contributes to the discussion on the relative importance of ERFs and GMMs in the overall uncertainty affecting seismic hazard estimates. The GMMs adopted in MPS19 were selected according to statistical criteria and elicitation procedures (Lanzano et al., 2020). We did not test the single ERFs (or branches) of MA4 with statistical procedures, but the mean seismic rates and the associated uncertainty were positively checked against 395 observations (i.e. number of earthquakes occurred in the last centuries) before entering in MPS19 (see Meletti et al., 2021 for details). In our opinion, however, trimming ERFs according to their performance against observations contributes to reducing the epistemic uncertainty, but could result in a selection of models that is only guided by the earthquake occurrence realization observed in the past.

400 **Author contributions.** FV wrote the draft of the paper, prepared the codes for the analysis and run the hazard calculations. All the Authors contributed to design the boundaries of ZS16, to revise seismic hazard results and to write the final version of the manuscript.

References

Albarello D., Camassi R., and Rebez A.: Detection of space and time heterogeneity in the completeness of a seismic catalogue 410 by a statistical approach: an application to the Italian area. Bull. Seismol. Soc. Am., 91, 1694–1703, https://doi.org/10.1785/0120000058, 2001.

Basili, R., Valensise, G., Vannoli, P., Burrato, P., Fracassi, U., Mariano, S., and Tiberti M.M.: The Database of Individual Seismogenic Sources (DISS), version 3: summarizing 20 years of research on Italy's earthquake geology. Tectonophysics 453, 1/4, 20-43. doi: 10.1016/j.tecto.2007.04.014, 2008.

415 Bernardi, F., Braunmiller, J., Kradolfer, U., and Giardini, D.: Automatic regional moment tensor inversion in the European-Mediterranean region, Geophys. J. Int., 157, 703–716, 2004.

Billi, A., Presti D., Orecchio, B., Faccenna, C., and Neri G.: Incipient extension along the active convergent margin of Nubia in Sicily, Italy: the Cefalu-Etna seismic zone. - Tectonics, 29, TC4026, doi:10.1029/2009TC002559, 2010.

Bindi, D., Massa, M., Luzi, L., Ameri, G., Pacor, F., Puglia, R., and Augliera, P.: Pan-European ground-motion prediction
420 equations for the average horizontal component of PGA, PGV, and 5 %-damped PSA at spectral periods up to 3.0 s using the RESORCE dataset. Bull Earthq Eng 12(1):391–430, 2014.

Bindi, D., Pacor, F., Luzi, L., Puglia, R., Massa, M., Ameri, G., and Paolucci, R.: Ground motion prediction equa-tions derived from the Italian strong motion database. Bull Earthq Eng 9(6):1899–1920, 2011

Boncio, P., Tinari, D.P., Lavecchia, G., Visini, F., and Milana, G.: The instrumental seismicity of the Abruzzo Region in
425 Central Italy (1981-2003): seismotectonic implications, Ital. J. Geosci. (Boll.Soc.Geol.It.), 128, 367-380, 2009.

Boncio, P., Lavecchia, G., and Pace, B.: Defining a model of 3D seismogenic sources for seismic hazard assessment applications: The case of central Apennines (Italy), Journal of Seismology, 8, 407-425, 2004.

Catalano, S., Romagnoli, G., and Tortorici, G.: Kinematics and dynamics of the Late Quaternary rift-flank deformation in the Hyblean Plateau (SE Sicily). Tectonophysics, 486 pp.1–14. ISSN: 0040-1951, doi:
430 10.1016/Tectonophysics, 486 pp.1–14. ISSN: 0040-1951, doi: 10.1016/j.tecto.2010.01.013,2010.

Cauzzi, C., Faccioli, E., Vanini, M., and Bianchini, A.: Updated predictive equations for broadband (0.01−10 s) horizontal response spectra and peak ground motions, based on a global dataset of digital acceleration records. Bull Earthq Eng. https ://doi.org/10.1007/s1051 8-014-9685-y, 2015.

CNR, P.F. GEODINAMICA: Structural Model of Italy 1:500.000 and Gravity Map, Quad. Ric. Sci., 3 (114), S.EL.CA.,
435 Firenze, 1990.

Collettini, C. and Barchi, M.R.: A Low Angle Normal Fault in the Umbria Region (Central Italy): A Mechanical Model for the Related Microseismicity. Tectonophysics, 359, 97-115. https://doi.org/10.1016/S0040-1951(02)00441-9, 2002.

Coppersmith, K. J., and Youngs, R. R.: Capturing uncertainty in probabilistic seismic hazard assessments within intraplate tectonic en-vironments, in Proceedings of the Third U.S. National Conference on Earthquake Engineering, Vol. 1, 301–312,
440 1986.

Danciu, L., Nandan, S., Reyes, C., Basili, R., Weatherill, G., Beauval, C., Rovida, A., Vilanova, S., Sesetyan, K., Bard, P-Y., Cotton, F., Wiemer, S., and Giardini, D.: The 2020 update of the European Seismic Hazard Model: Model Overview. EFEHR Technical Report 001, v1.0.0, https://doi.org/10.12686/a15, 2021.

Danciu, L., Şeşetyan, K., Demircioglu, M., et al.: The 2014 Earthquake Model of the Middle East: seismogenic sources. Bull
445 Earthquake Eng 16, 3465–3496, https://doi.org/10.1007/s10518-017-0096-8, 2018.

Delacou, B., Sue, C., Champagnac, J.D., and Burkhard, M.: Present-day geodynamics in the bend of the Western and Central Alps as constrained by earthquake analysis. Geophys J Int 158:753–774, 2004.

Della Vedova, B., Bellani, S., Pellis, G., and Squarci, P.: Deep temperatures and surfaceheat flow density distribution. In: Vai, G.B., Martini, P. (Eds.), Anatomy of an Orogen: The Apennines and Adjacent Mediterranean Basins. Kluwer Academic

450   Publishers, Dordrecht, Netherlands, pp. 65–76, 2001.

Devoti, R., D'Agostino, N., Serpelloni, E., Pietrantonio, G., Riguzzi, F., et al.: A Combined Velocity Field of the Mediterranean Region. Annals of Geophysics, 60 (2), 2017.

Di Stefano, R., Bianchi, I., Ciaccio,M.G., Carrara,G., and Kissling, E.: Three-dimensional Moho topography in Italy: new constraints from receiver functions and controlled source seismology, Geochem. Geophy. Geosyst, 2011, vol. 12 (9) Q09006,

455   doi:10.1029/2011GC003649, 2011.

DISS Working Group: Database of Individual Seismogenic Sources (DISS), Version 3.2.1: A compilation of potential sources for earthquakes larger than M 5.5 in Italy and surrounding areas, Istituto Nazionale di Geofisica e Vulcanologia, doi: https://doi.org/10.6092/INGV.IT-DISS3.2.1, 2018.

Ekström, G., M. Nettles, and Dziewonski, A. M.: The global CMT project 2004-2010: Centroid-moment tensors for 13,017

460   earthquakes, Phys. Earth Planet. Inter., 200-201, 1-9, 2012. doi:10.1016/j.pepi.2012.04.002, 2012.

Faure Walker, J. P. et al.: Relationship between topography, rates of extension and mantle dynamics in the actively-extending Italian Apennines. Earth and Planetary Science Letters 325–326, 76–84 , 2012.

Faure Walker, J. P., Roberts, G., Sammonds, P., and Cowie, P.: Comparison of earthquake strains over 100 and 10,000 year timescales: insights into variability in the seismic cycle in the central Apennines, Italy. J. Geophys. Res. 115, B10418,

465   https://doi.org/10.1029/2009JB006462, 2010.

Gardner, J.K., and Knopoff L.: Is the sequence of earthquakes in Southern California, with aftershocks removed, Poissonian? Bull. Seismol. Soc. Am. 64, 5, 1363-1367, 1974.

Gasperini, P., Bernardini, F., Valensise, G., and Boschi, E.: Defining seismogenic sources from historical earthquake felt reports. Bull Seismol Soc Am 89:94–110, 1999.

470   Gasperini, P., Lolli, B., and Vannucci, G.: Empirical calibration of local magnitude data sets versus moment magnitude in Italy. Bull Seismol Soc Am 103:2227–2246, 2013.

Gasperini, P., Lolli, B., Vannucci, G., and Boschi, E.: A comparison of moment magnitude estimates for the European— Mediterranean and Italian region. Geophys J Int 190:1733–1745, 2012.

Gasperini, P., Vannucci, G., Tripone, D., and Boschi, E.: The location and sizing of historical earthquakes using the attenuation

475   of macroseismic intensity with distance. Bull Seismol Soc Am 100:2035–2066, 2010.

Gasperini, P., Lolli, B., and Vannucci, G.: Catalogueue of Mw magnitudes for the Italian area, 1981-2015. MPS16 Project Internal report., 2016.

Giardini, D.: The Global Seismic Hazard Assessment Program (GSHAP)—1992/1999, 1999.

Kulkarni, R.B., Youngs, R.R., and Coppersmith, K.J.: Assessment of confidence intervals for results of seismic hazard

480   analysis, in Pro-ceedings of the Eighth World Conference on Earthquake Engineering, San Francisco, Vol. 1, 263–270, 1984.

Lanzano, G., and Luzi, L.: A ground motion model for volcanic areas in Italy. Bull Earthq Eng. https ://doi.org/10.1007/s1051 8-019-00735 -9, 2020.

Lanzano, G., Luzi, L., D'Amico, V., Pacor, F., Meletti, C., Marzocchi, W., Rotondi, R. and Varini, E.: Ground Motion Models for the new seismic hazard model of Italy (MPS19): selection for active shallow crustal regions and subduction zones, Bull.

485   Earthq. Eng., 18, 3487–3516, doi:10.1007/s10518-020-00850-y, 2020.

Lavecchia, G., De Nardis, R., Visini, F., Ferrarini, F., Barbano, M.S.: Seismogenic evidence of ongoing compression in eastern-central Italy and mainland Sicily: a comparison. Italian Journal of Geosciences (Boll Soc Geol It), 126, 209-222, 2007a.

Lavecchia, G., Ferrarini, F., de Nardis, R., Visini, F.,and Barbano, M.S.: Active thrusting as a possible seismogenic source in Sicily (southern Italy): Some insights from integrated structural-kinematic and seismological data, Tectonophysics, 445, 145–

490   167, doi:10.1016/j.tecto.2007.07.007, 2007b.

Lolli, B., Gasperini, P., and Rebez, A.: Homogenization of magnitude estimates in terms of Mw of Italian earthquakes occurred before 1981. Bull Seismol Soc Am 108:481–492. https://doi.org/10.1785/0120170114, 2018.

Lolli, B., Gasperini, P., and Vannucci, G.: Empirical conversion between teleseismic magnitudes (mb and Ms) and moment magnitude (Mw) at the global, Euro-Mediterranean and Italian scale. Geophys J Int 199:805–828.

495   https://doi.org/10.1093/gji/ggu264, 2014.

Lolli, B., Gasperini, P., and Vannucci, G.: Erratum: Empirical conversion between teleseismic magnitudes (mb and Ms) and moment magnitude (Mw) at the global, Euro-Mediterranean and Italian scale. Geophys J Int 200:199. https://doi.org/10.1093/gji/ggu385, 2015.

Lolli, B., Randazzo, D., Vannucci, G., and Gasperini, P.: The Homogenized Instrumental Seismic Catalogue (HORUS) of

500   Italy from 1960 to Present, Seismol. Res. Lett. 91 3208–3222, doi:10.1785/0220200148, 2020.

Maesano, F. E., Tiberti, M.M, and Basili, R.: The Calabrian Arc: three-dimensional modelling of the subduction interface. Sci Rep 7, 8887 (2017). https://doi.org/10.1038, 2017.

Mariucci, M.T., and Montone, P.: Database of Italian present-day stress indicators, IPSI 1.4. Sci. Data 7, 1–11. https://doi.org/10.1038/s41597-020-00640-w, 2020.

505   Mastrolembo, B., Serpelloni, E., Argnani, A., Bonforte, A., Burgmann, R., Anzidei, M., Baldi, P., and Puglisi, G.: Fast geodetic strain-rates in eastern Sicily (southern Italy): New insights into block tectonics and seismic potential in the area of the great 1693 earthquake. Earth and Planetary Science Letters. 404. 10.1016/j.epsl.2014.07.025, 2014.

Meletti, C., Patacca, E., and Scandone, P.: Construction of a seismo- tectonic model: The case of Italy, Pure Appl. Geophys. 157, 11–35, 2020.

510   Meletti, C., Galadini, F., Valensise, G., Stucchi, M., Basili, R., Barba, S., Vannucci, G., and Boschi, E.: A seismic source model for the seismic hazard assessment of the Italian territory. Tectonophysics 450 (1), 85-108. doi:10.1016/j.tecto.2008.01.003, 2008.

Meletti, C., Marzocchi, W., D'Amico, V., Lanzano, G., Luzi, L., Martinelli, F., Pace, B., Rovida, A., Taroni, M., Visini, F., and the MPS19 Working Group: The new Italian Seismic Hazard Model (MPS19). Annals of Geophysics, 64 (1),

515 doi:10.4401/ag-8579, 2021.

National Research Council (US): Panel on Seismic Hazard Analysis, Keiiti Aki, National Research Council (US). Committee on Seismology, National Research Council (US). Board on Earth Sciences, National Research Council (US). Commission on Physical Sciences, Mathematics and Resources. Probabilistic Seismic Hazard Analysis. National Academies, 1988.

Papanikolaou, I.D., and Roberts, G.P.: Geometry, Kinematics and deformation rates along the active normal fault system in

520 the southern Apennines: implications for fault growth. J. Struct. Geol., 29, pp. 166-188, 2007.

Pondrelli, S., and Salimbeni, S.: Regional Moment Tensor Review: An Example from the European–Mediterranean Region. In Encyclopedia of Earthquake Engineering (pp. 1–15). Springer Berlin Heidelberg. https://doi.org/10.1007/978-3-642-36197-5_301-1, 2015.

Pondrelli, S., Salimbeni, S., Ekström, G., Morelli, A., Gasperini, P., and Vannucci G.: The Italian CMT dataset from 1977 to

525 the present. Phys. Earth Planet. Int., 159, 286–303, https://doi.org/10.1016/j.pepi.2006.07.008, 2006.

Pondrelli, S., Visini, F., Rovida, A., D'Amico, V., Pace, B., and Meletti, C.: Style of faulting of expected earthquakes in Italy as an input for seismic hazard modeling, Nat. Hazards Earth Syst. Sci., 20, 3577–3592, https://doi.org/10.5194/nhess-20-3577-2020, 2020.

Rovida, A., Locati, M., Camassi, R., Lolli, B., and Gasperini, P.: CPTI15, the 2015 version of the Parametric Catalogueue of

530 Italian Earthquakes. Istituto Nazionale di Geofisica e Vulcanologia. doi: https://doi.org/10.6092/INGV.IT-CPTI15, 2016.

Rovida, A., Locati, M., Camassi, R., Lolli, B., and Gasperini, P.: The Italian earthquake catalogueue CPTI15. Bulletin of Earthquake Engineering, 18, 2953–2984 (2020). doi: https://doi.org/10.1007/s10518-020-00818-y, 2020.

Saul, J., Becker, J., and Hanka, W.: Global moment tensor computation at GFZ Potsdam, AGU 2011 Fall Meeting, San Francisco, USA, abstract ID. S51A-2202, 2011.

535 Solarino S., and Cassinis R.: Seismicity of the upper lithosphere and its relationships with the crust in the Italian region. Bollettino di Geofisica teorica ed applicata, 48, 2, 99-115, 2007.

SSHAC (Senior Seismic Hazard Analysis Committee): Recommendations for probabilistic seismic haz-ard analysis: guidance on uncertainties and use of experts. Report NUREG- CR- 6372, U.S. Nuclear Regulatory Commission, Washington D.C., 1997.

540 Stucchi, M., Albini, P., Mirto, C., Rebez, A.: Assessing the completeness of Italian historical earthquake data. Ann Geophys 47, 659-674, 2004.

Stucchi, M., Meletti, C., Montaldo, V., Crowley, H., Calvi, G.M., and Boschi, E.: Seismic hazard assessment (2003-2009) for the Italian building code. Bulletin of the Seismological Society of America, 101, 1885-1911, 2011.

Sue, C., Delacou, B., Champagnac, JD., et al.: Extensional neotectonics around the bend of the Western/Central Alps: an

545 overview. Int J Earth Sci (Geol Rundsch) 96, 1101–1129. https://doi.org/10.1007/s00531-007-0181-3, 2007.

Tesson, J., Pace, B., Benedetti, L., Visini, F., Delli Rocioli, M., Arnold, M., Aumaître, G., Bourlès, D. L., and Keddadouche, K.: Seismic slip history of the Pizzalto fault (central Apennines, Italy) using in situ-produced36Cl cosmic ray exposure dating and rare earth element concentrations. Journal of Geophysical Research: Solid Earth, 121 (3). 1983-2003 doi:10.1002/2015jb012565, 2016.

550   Valentini, A., Visini, F., and Pace, B.: Integrating faults and past earthquakes into a probabilistic seismic hazard model for peninsular Italy, Nat. Hazards Earth Syst. Sci., 17, 2017–2039, https://doi.org/10.5194/nhess-17-2017-2017, 2017.

Vannucci, G. and Gasperini, P.: The new release of the database of Earthquake Mechanisms of the Mediterranean Area (EMMA Version 2), Ann. Geophys., 47, 307–334, 2004.

Vilanova, S. P., Nemser, E. S., Besana-Ostman, G. M., Bezzeghoud, M., Borges, J. F., Brum da Silveira, A., Cabral, J.,
555   Carvalho, J., Cunha, P. P., Dias, R. P., Madeira, J., Lopes, F. C., and Oliveira, C.: Incorporating Descriptive Metadata into Seismic Source Zone Models for Seismic-Hazard Assessment: A Case Study of the Azores-West Iberian Region. Bulletin of the Seismological Society of America, 04(3), DOI:10.1785/0120130210, 2014.

Visini, F, Pace, B, Meletti, C, Marzocchi, et al.: Earthquake Rupture Forecasts for the MPS19 Seismic Hazard Model of Italy. Ann. Geophys.;64(2):SE220, 2021.

560   Visini, F.: Seismic crustal deformation in Southern Apennines of Italy. Italian Journal of Geosciences, 131, 187-204, doi: 10.3301/IJG.2011.31, 2012.

Visini, F., De Nardis, R., Lavecchia, G.: Rates of active compressional deformation in central Italy and Sicily: evaluation of the seismic budget. International Journal of Earth Sciences, 99 (1), 243-264, doi: 10.1007/s00531-009-0473-x, 2010.

Weichert, D.H.: Estimation of the earthquake recurrence parameters for unequal observation periods for different magnitudes.
565   Bulletin of the Seismological Society of America 70 (4), 1337-1346, 1980.

Wells, D. L., and Coppersmith, K.J.: New empirical relationships among magnitude, rupture length, rupture width, rupture area, and surface displacement. Bulletin of the Seismological Society of America, 84(4), 974–1002, 1994.

Woessner, J., Danciu, L., Giardini, D. Crowley, H., Cotton, F., et al.: The 2013 European Seismic Hazard Model - Key Components and Results. Bulletin of Earthquake Engineering, 13, 3553-3596, doi: 10.1007/s10518-015-9795-1, 2015.
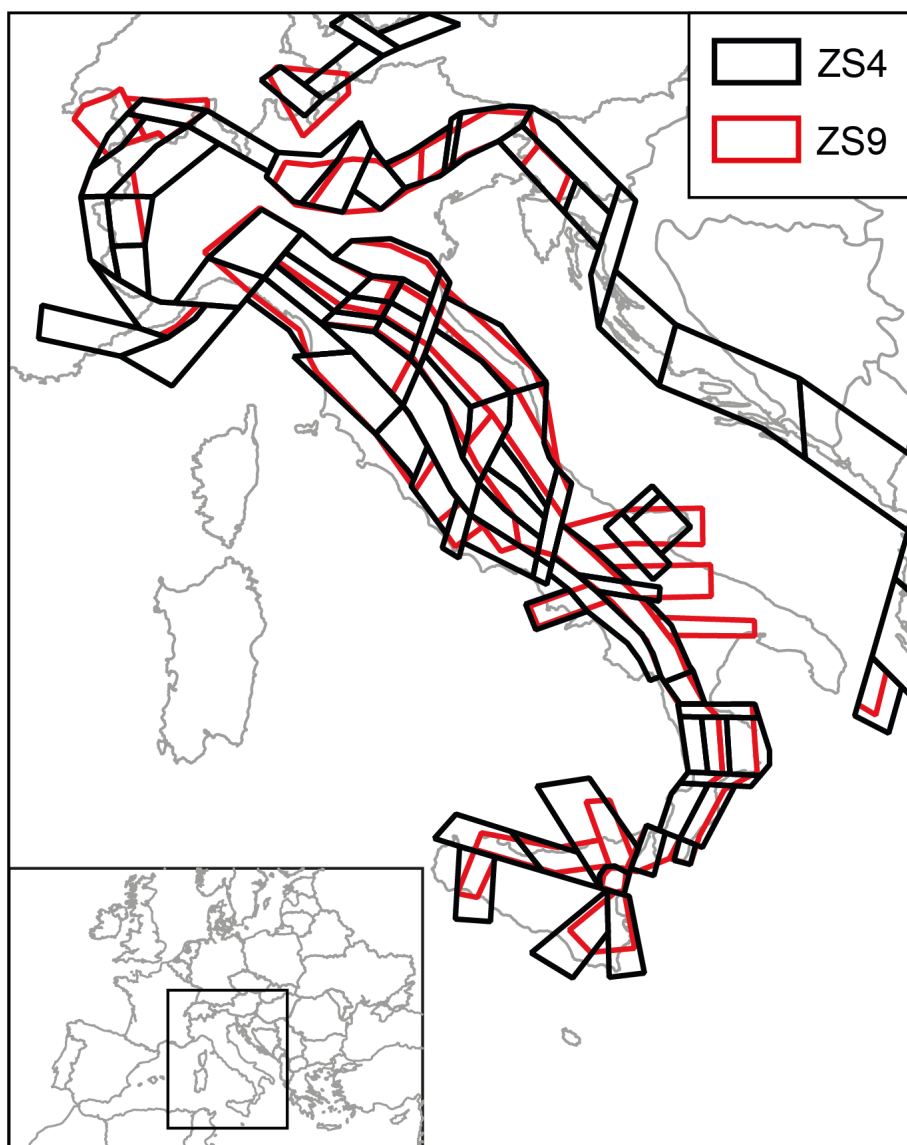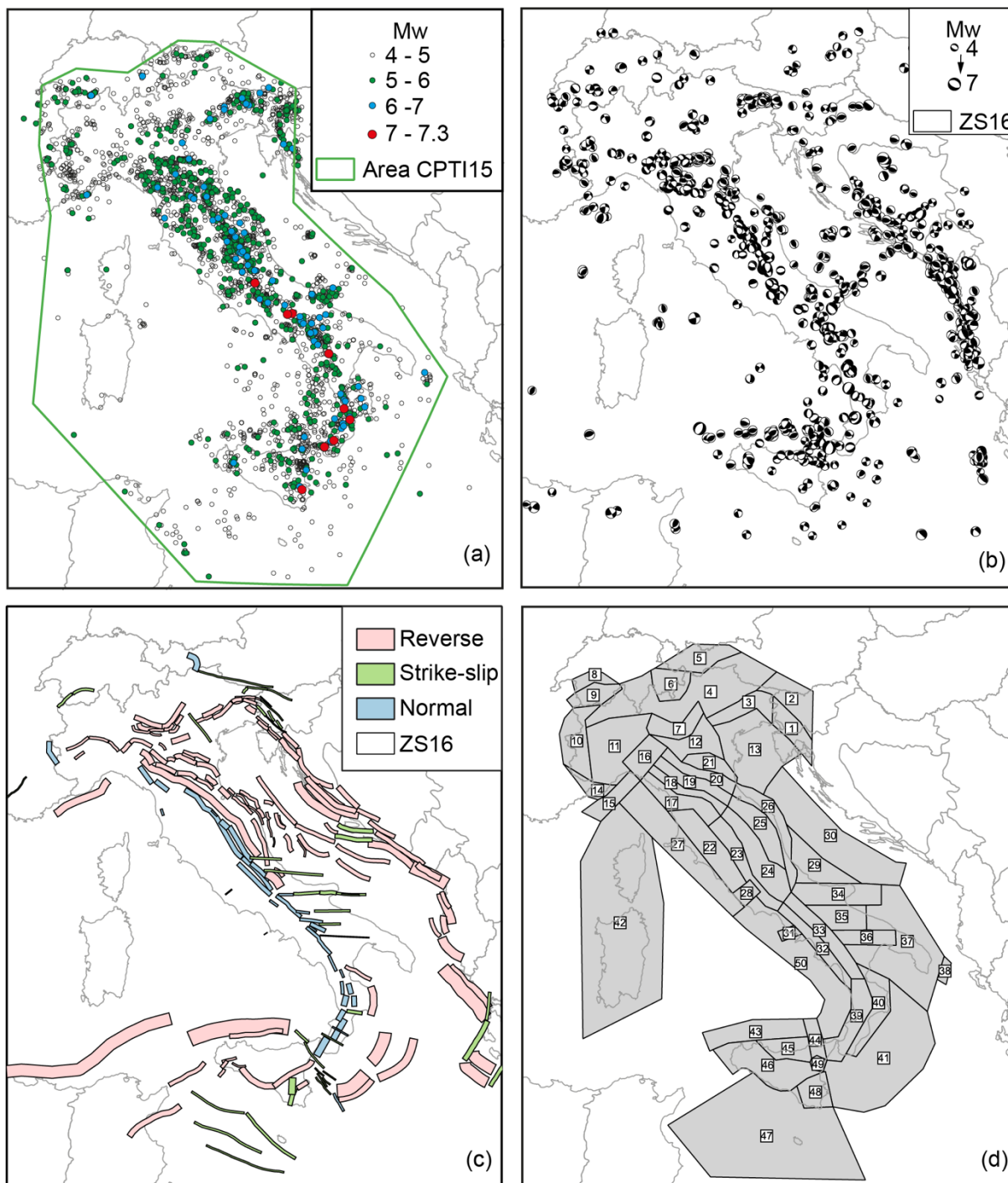
570

Figure 1. Comparison of ZS4 by Meletti et al. (2000) and ZS9 by Meletti et al. (2008). ZS9 is the seismotectonic zoning of the current Italian seismic hazard model (MPS04) by Stucchi et al. (2011).

Figure 2. Main datasets (a, b, c) used to build the ZS16 (d) seismotectonic zoning. a) Earthquake epicenters from the CPTI15 catalogue (the green polygon represents the area of reliability of the CPTI15, as described by Rovida et al., 2016; 2020); b) focal mechanisms of earthquakes with Mw≥4 (Pondrelli et al., 2020); c) Composite Seismogenic Sources from the DISS3.2.1 database; d) Seismotectonic zoning ZS16 proposed in this study.
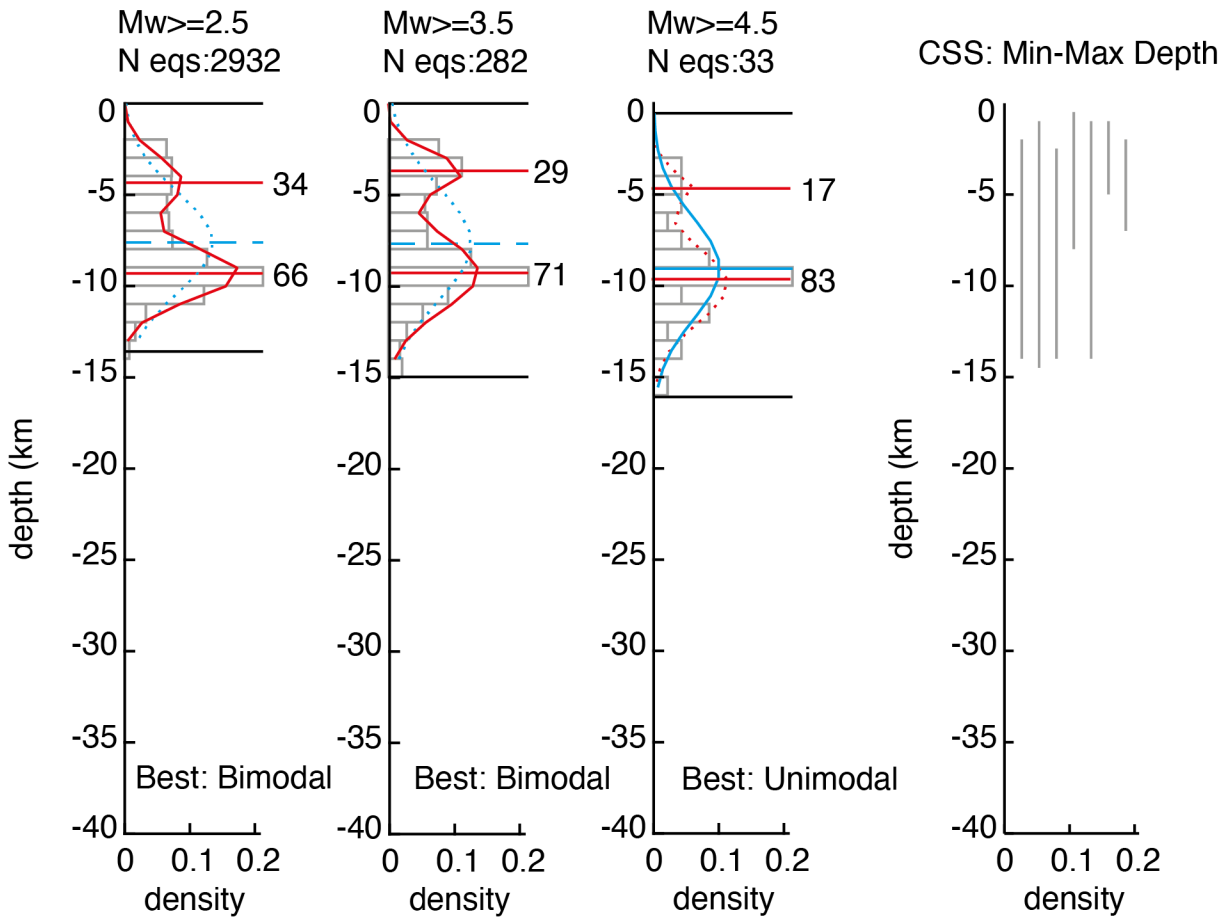
Figure 3. Hypocentral depth distributions (grey bars) for different threshold magnitudes (reported on top of each panel along with the number of considered earthquakes) for zone #24. Black lines correspond to the 5th and 95th percentiles, assumed as upper/lower seismogenic depths; blue curve and line represent the unimodal distribution and its modal value; red curve and lines represent the bimodal distribution and its two modal values. Solid lines indicate the best model between uni- and bi-modal distributions, dashed lines the other model. The right panel shows the depth ranges of the composite seismogenic sources (CSS) of DISS 3.2.1 inside the area.
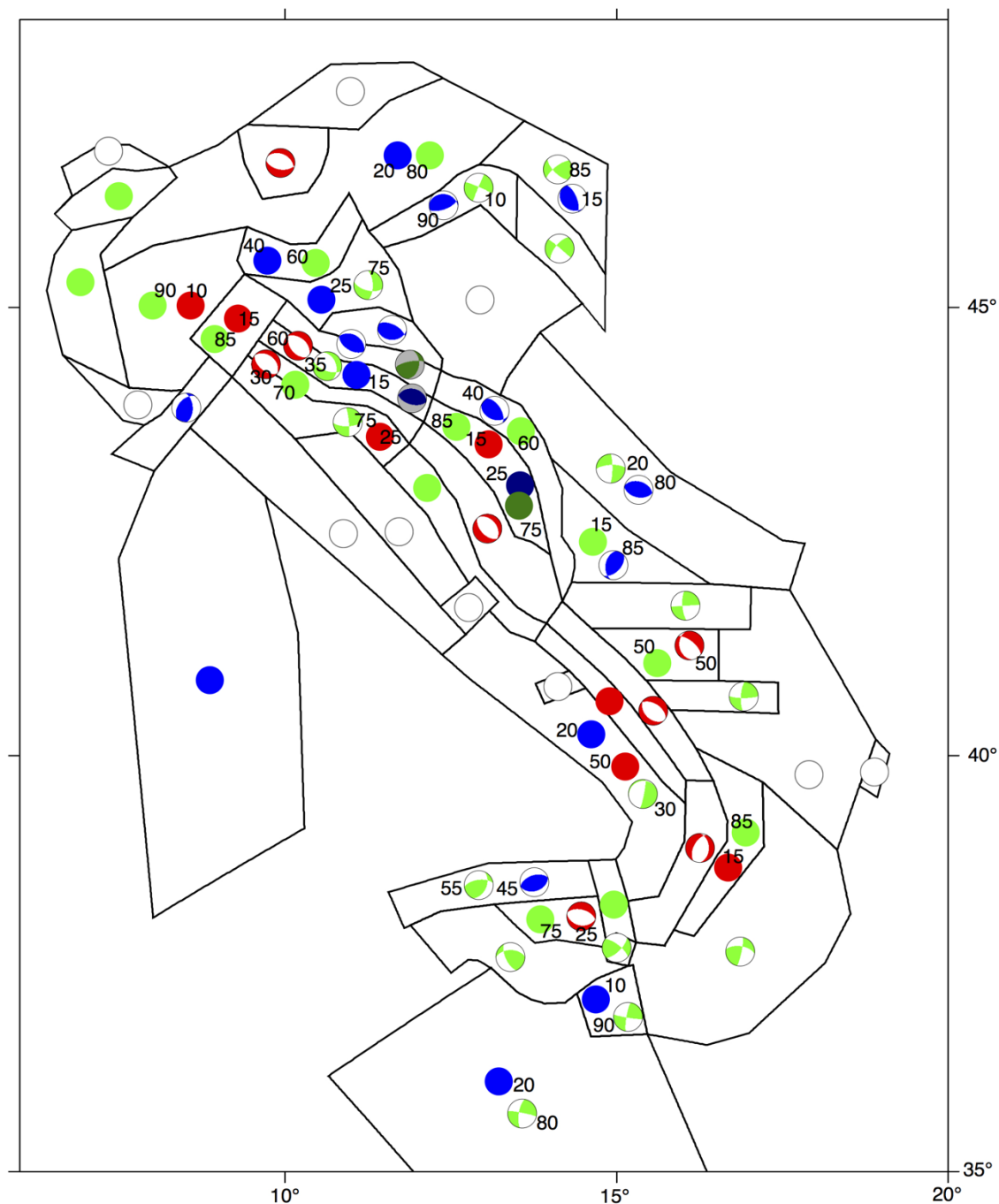
Figure 4. Expected style of faulting for each area source (modified from Pondrelli et al., 2020). Full circles represent random seismic sources and white circles represent 100 % random while blue, red, and green circles correspond to reverse, normal, and strike-slip random sources, respectively. Cumulative focal mechanisms colors follow the same criteria. Focal mechanisms with a grey background or circles with darker colors are the sources for deeper layers. Black numbers are the percentages of contribution to the final source when their sum is the expected style of faulting.
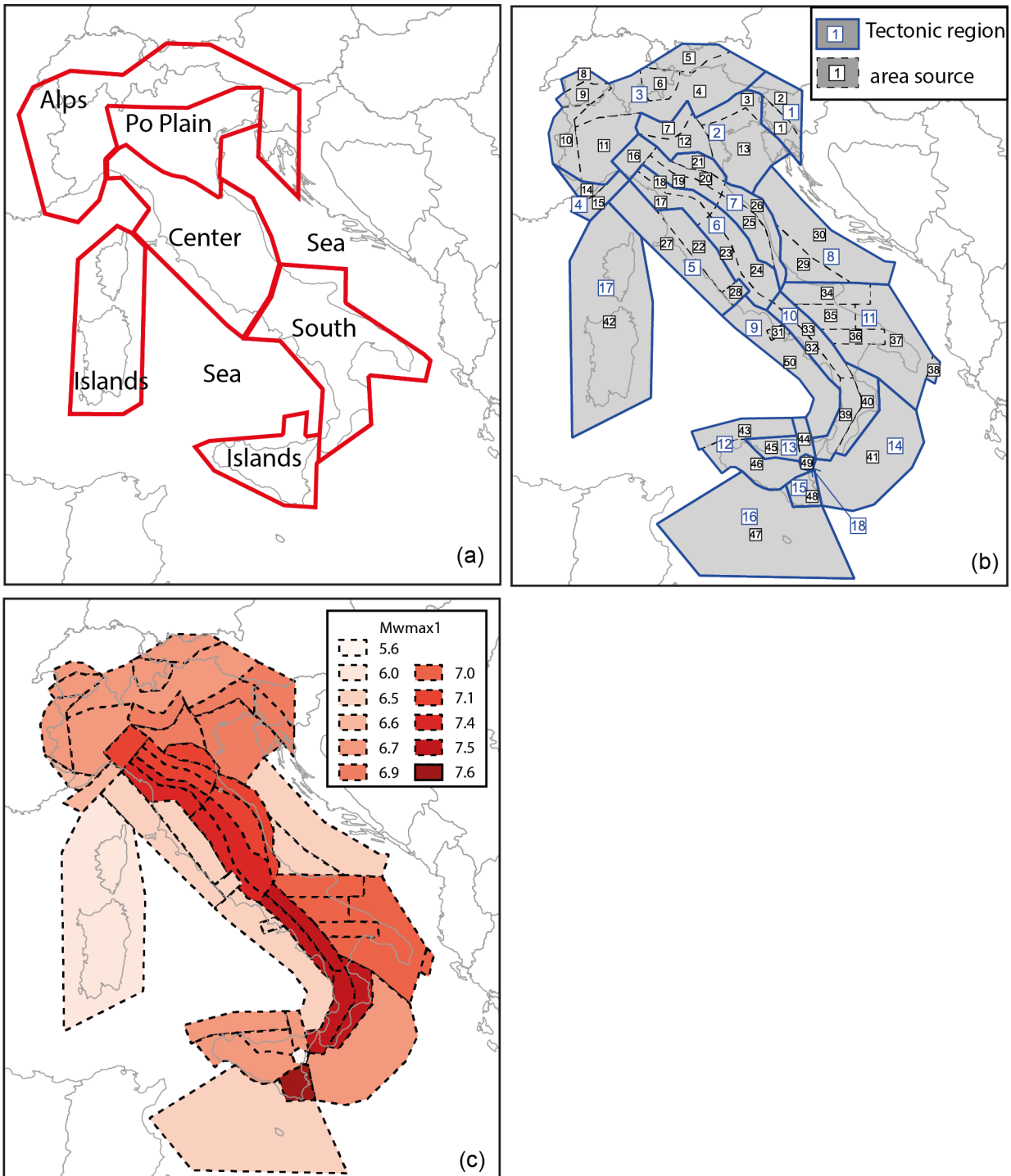
Figure 5. a) Macro-regions adopted for evaluating the completeness time intervals for the earthquake catalogue; **b)** Tectonic regions (blue polygons) used to calculate β overlapped to the ZS16 area sources (dashed black polygons); **c)** Map of the values of Mwmax1, Mwmax2 = Mwmax1 + 0.3.
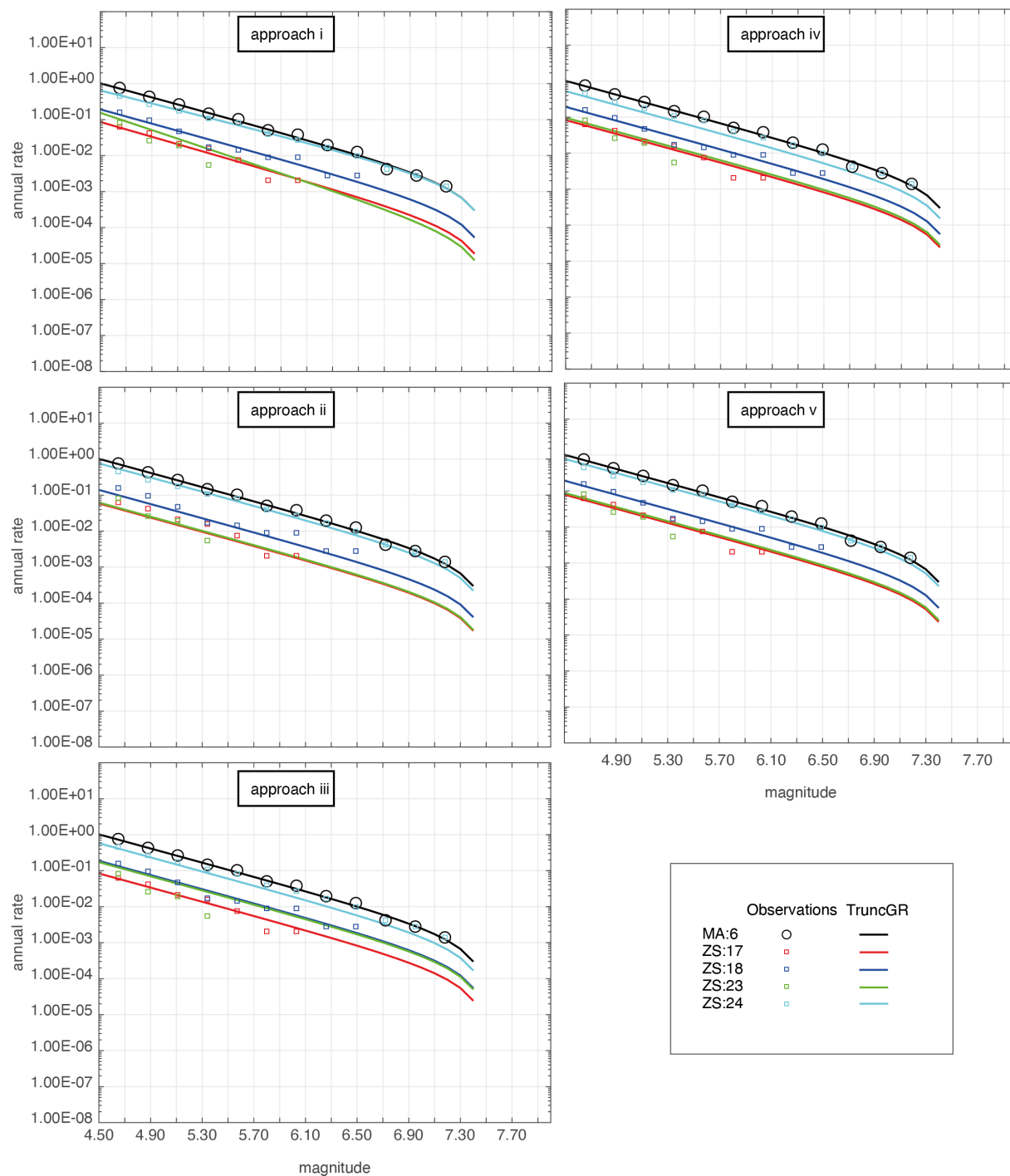
Figure 6. Example of the frequency-magnitude distributions calculated directly for the area sources #17, #18, #23 and #24 (method 1) and the distributions calculated for the macroarea #6 and partitioned to the mentioned sources (methods from 2 to 5). The 4 source zones and the macroarea are shown in Figure 5b.
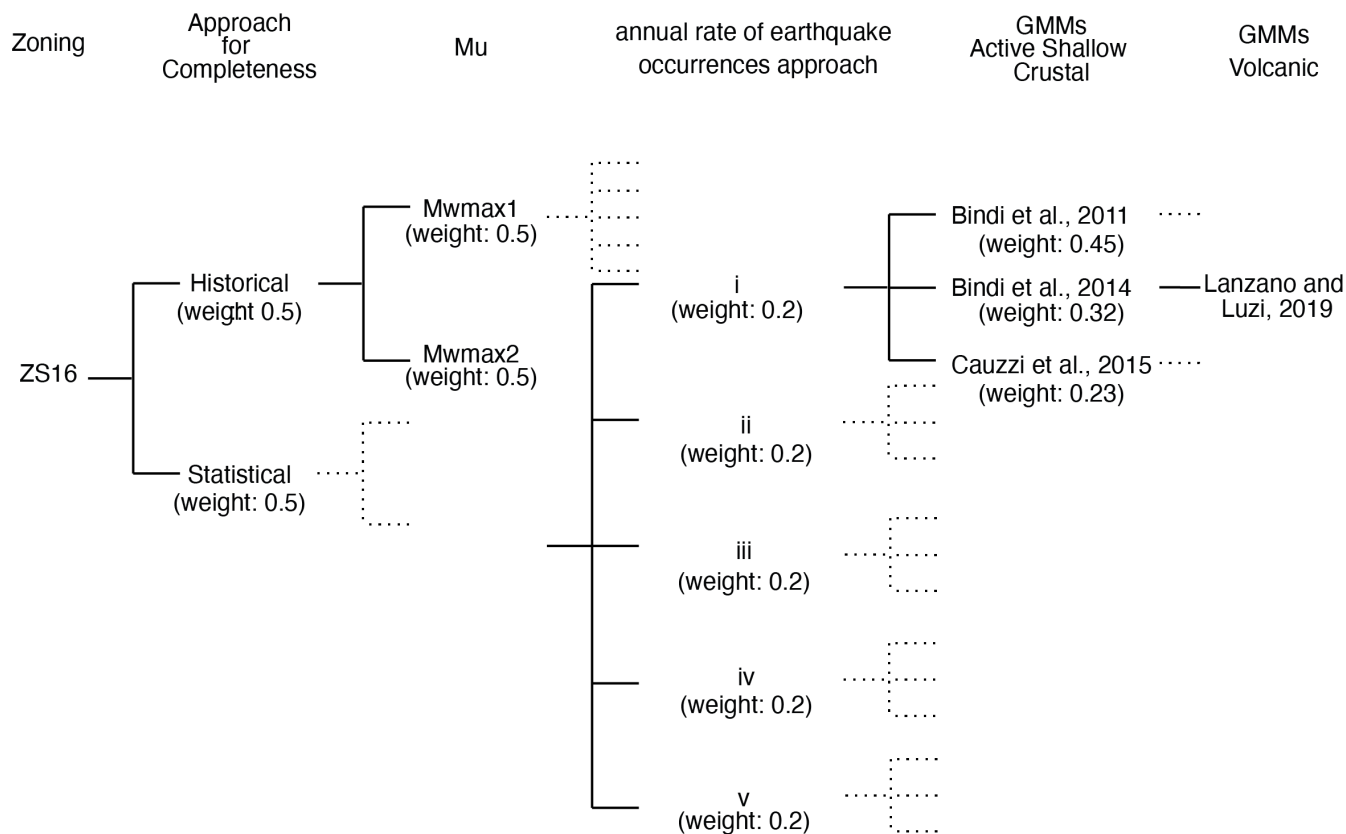
Natural Hazards
and Earth System
Sciences
Discussions
Open Access
EGU

Figure 7. The logic-tree scheme adopted in this study. "ZS16" is the seismotectonic zoning. The completeness time intervals for the CPTI15 catalogue were defined according to the historical approach of Stucchi et al. (2004; 2011) and the statistical method of Albarello et al. (2001). Mu "Mwmax1" and Mu "Mwmax2" are the two sets of values adopted for the maximum magnitude, described in Visini et al. (2021). Letters "i"-to-"v" identify the 5 approaches used to calculate the annual seismic rates (see section 3.34.). The last two nodes concern the GMMs used for active shallow crustal regions and volcanic areas.
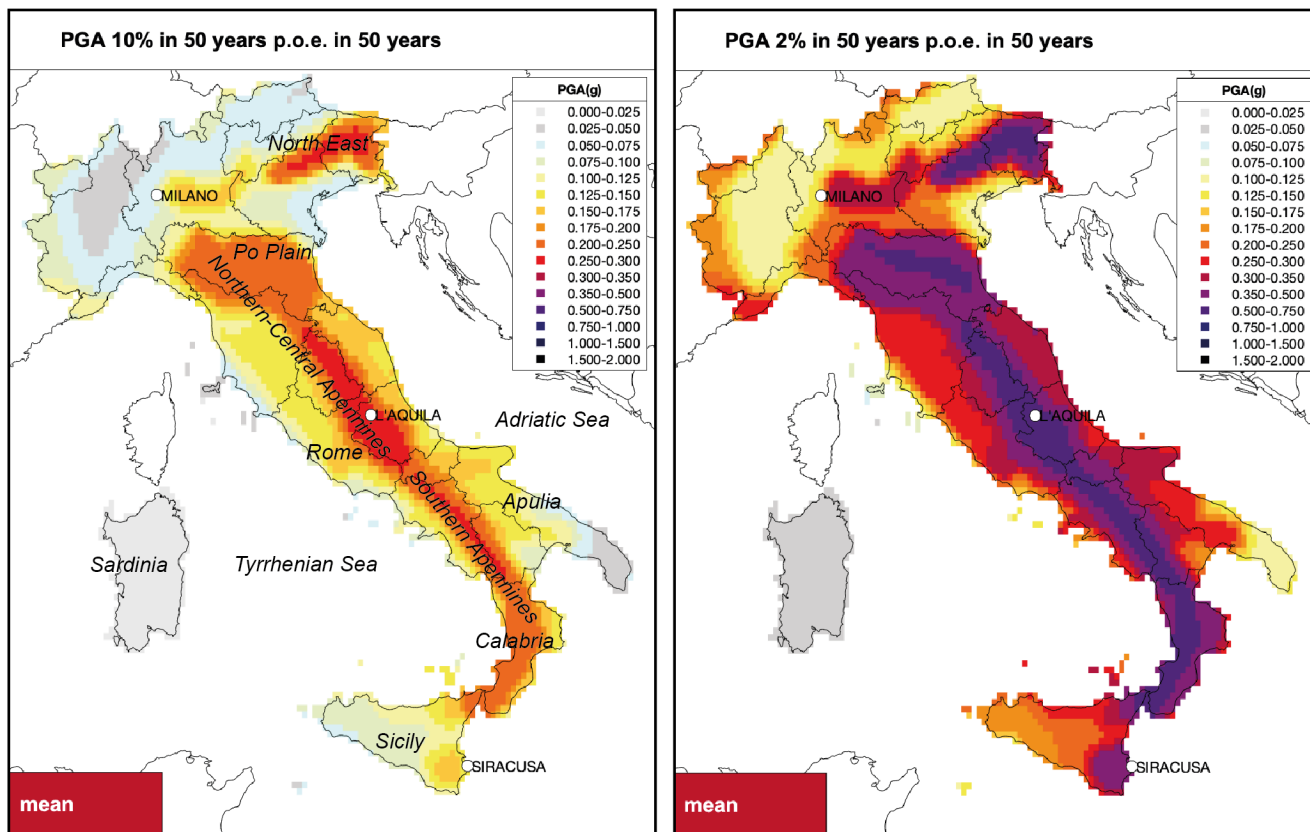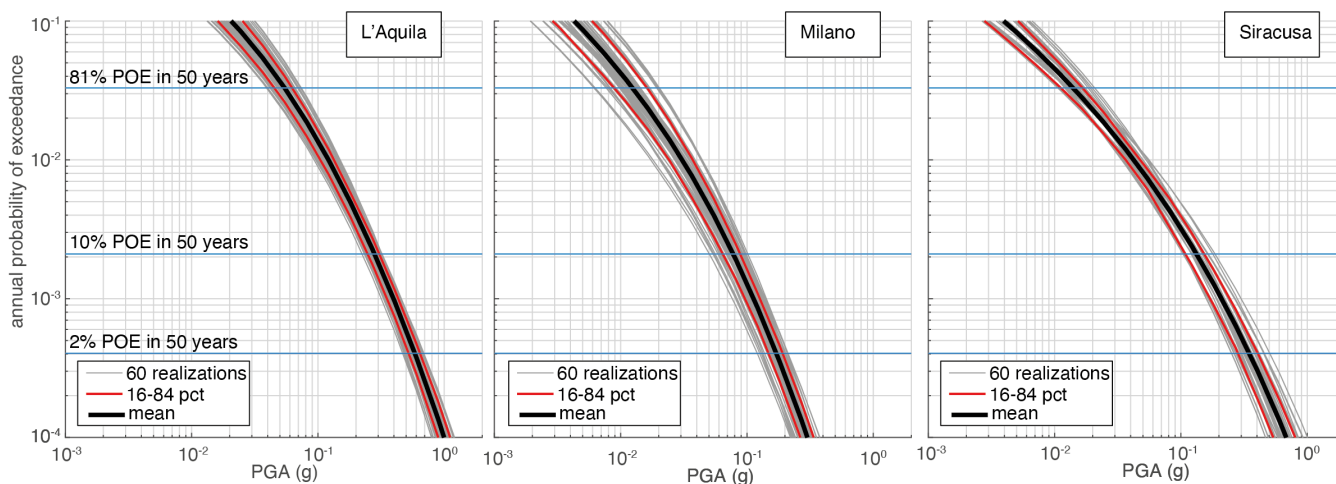
Figure 8. Maps of mean values of PGA at 10% (left) and 2% (right) probability of exceedance in 50 years. Locations of the 3 cities selected for detailed analyses are shown.

610

Figure 9. Hazard curves for PGA for the 3 selected cities. The curves represent: the mean hazard level (black line), the hazard resulting from each of the 60 branches (realizations, grey lines) and the uncertainties expressed through the 16th and 84th percentiles (red lines).
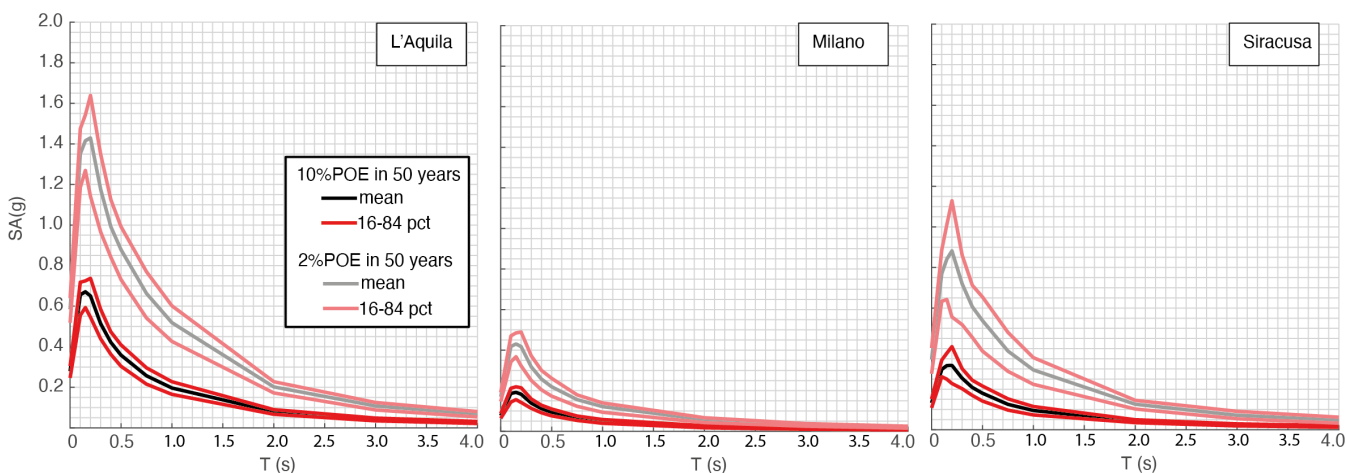
Figure 10 UHS for 10% (lower spectra) and 2% (upper spectra) probability of exceedance in 50 years for the 3 selected cities. The mean spectra and the 16th and 84th percentiles are reported.
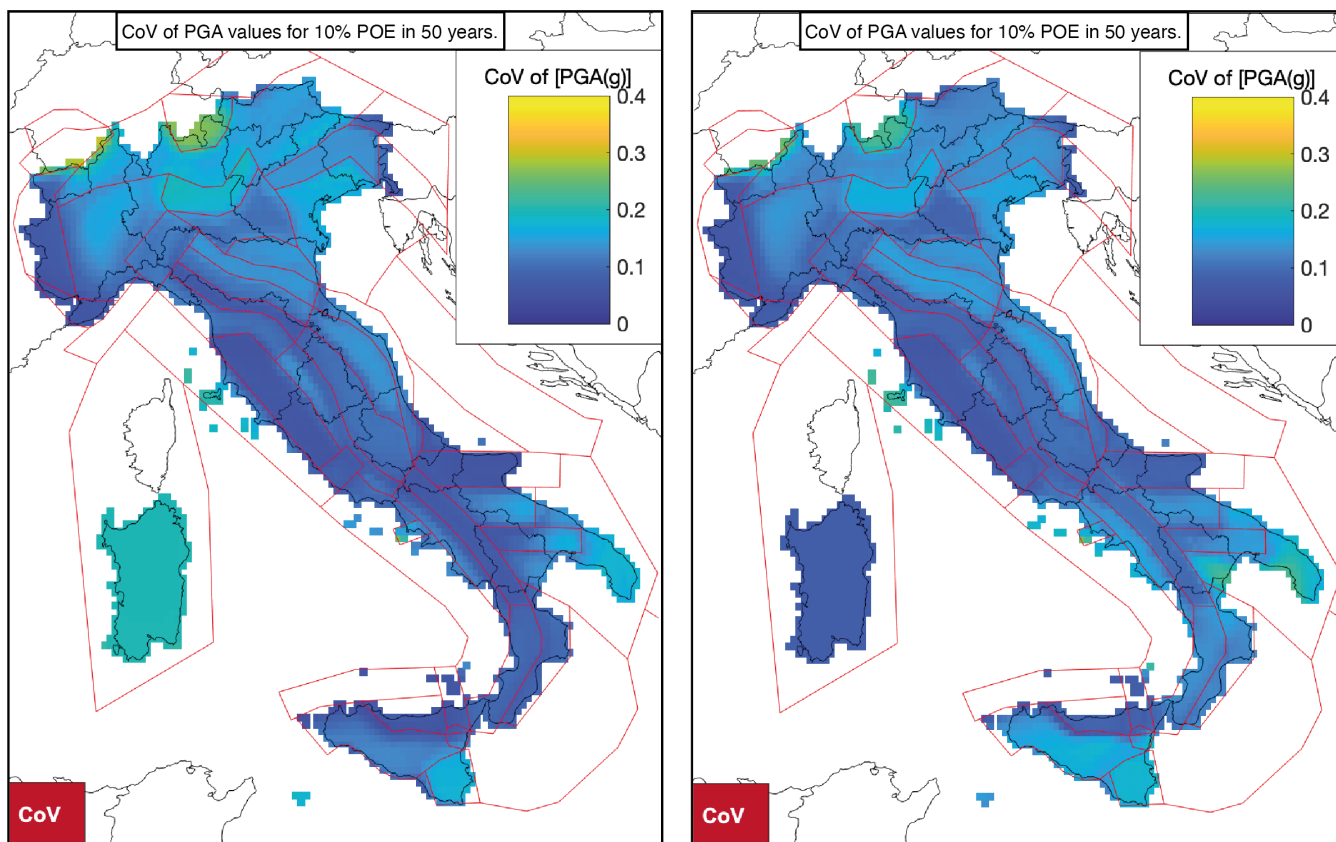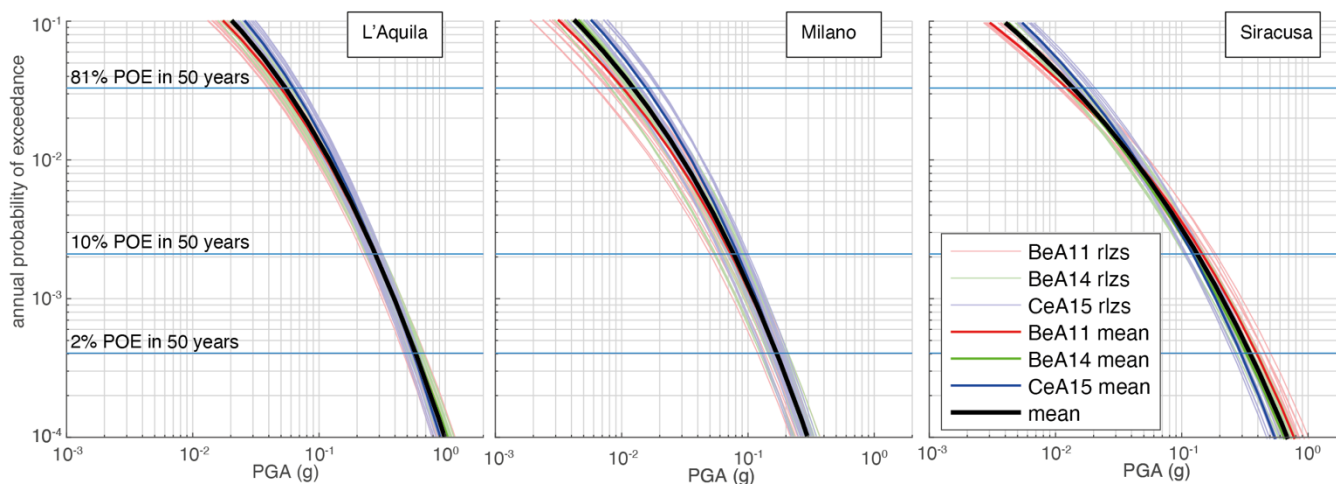
Figure 11. Spatial distribution of the coefficient of variation (CoV) of PGA values for 10% (left) and 2% (right) probabilities of exceedance in 50 years.

625

Figure 12. Hazard curves for PGA for the 3 selected cities. The curves represent: the mean hazard level (black line); the mean hazard level obtained as a weighted average of the realizations per each GMM and; the hazard resulting from each of the 60 branches (realizations, colored per GMM).

630
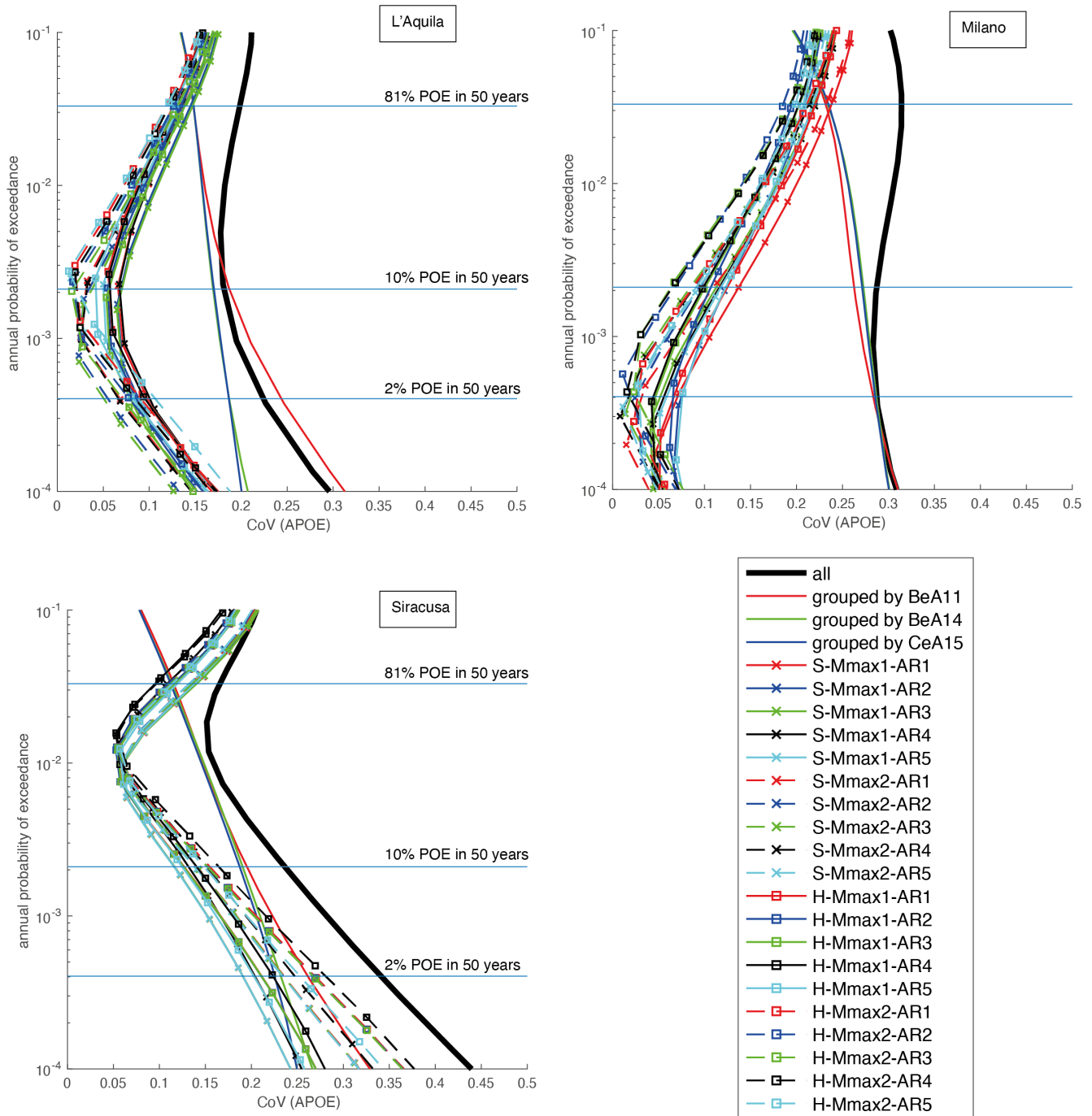
Figure 13. Magnitude of epistemic uncertainty in ERF and ground motion hazard estimates shown as CoV againt mean APOE.
635 **Branches that use the same GMM are shown with 3 solid lines without symbols, red, green and blue; branches that use the same approach for completeness estimate, maximum magnitude and seismic rates of the zones are shown by lines with symbols.**

Bin	Io	Mw	Alps	Po Plain	Center	South	Islands	Sea
1	4-5	3.96	1900	1950	1950	1950	1950	2002
2	5	4.19	1900	1836	1900	1895	1950	2002
3	5-6	4.42	1871	1836	1871	1895	1871	2002
4	6	4.65	1871	1836	1871	1895	1871	1984
5	6-7	4.88	1871	1836	1871	1895	1871	1984
6	7	5.11	1700	1530	1650	1787	1700	1984
7	7-8	5.34	1700	1530	1650	1787	1700	1984
8	8	5.57	1530	1530	1650	1787	1700	1963
9	8-9	5.80	1530	1300	1530	1787	1530	1963
10	9	6.03	1300	1300	1530	1530	1530	1963
11	9-10	6.26	1300	1100	1300	1530	1300	1963
12	10	6.49	1300	1100	1300	1400	1300	1963
13	10-11	6.72	1300	1100	1300	1400	1300	1963
14	11	6.95	1300	1100	1300	1400	1300	1963
15	11-12	7.18	1300	1100	1300	1400	1300	1963

Table 1. Completeness starting year for each I0/Mw bin and macro-region defined according to the historical approach. The Mw value is the center of each bin (0.23 Mw units).

640

Bin	Mw	Alps	Po Plain	Center	South	Islands	Sea
A	3.85	1870	1870	1880	1960	1890	1960
B	4.31	1870	1870	1880	1960	1890	1960
C	4.77	1850	1870	1880	1870	1870	1960
D	5.23	1810	1830	1790	1820	1680	1930
E	5.69	1530	1690	1750	1760	1600	1930
F	6.15	1490	1450	1580	1660	1500	1930
G	6.61	1490	1320	1580	1600	1500	1930
H	7.07	1490	1320	1580	1550	1500	1930
I	7.53	1490	1320	1580	1550	1500	1930

Table 2. Completeness starting year for each I0/Mw bin and macro-region defined according to the statistical approach. In order to have enough data in each bin, we adopted a double width with respect to the historical approach and then applied the results to the same bins of Table 1. The Mw value is the center of each bin (0.46 Mw units).

645